

DOE/ER/40561-311-INT97-00-162

Importance of the direct knockout mechanism in relativistic calculations for (γ, p) reactions*

J.I. Johansson

Department of Physics, University of Manitoba
Winnipeg, Manitoba, R3T 2N2

and

Institute for Nuclear Theory, University of Washington
Box 351550, Seattle, Washington, 98195-1550

and

H.S. Sherif

Department of Physics, University of Alberta
Edmonton, Alberta, Canada T6G 2J1

September 29, 2018

Abstract

Results of relativistic calculations of the direct knockout (DKO) mechanism for the photon induced removal of a proton from a target nucleus over a wide range of energies and nuclei are presented. Spectroscopic factors used in the calculations are fixed from consistent

*This work was supported in part by the Natural Sciences and Engineering Research Council of Canada.

analyses of the quasifree electron scattering process $(e, e'p)$. The results indicate that within the uncertainties of the model, the knockout contributions are generally close to the experimental data for missing momenta below ≈ 500 MeV/ c . This is in disagreement with nonrelativistic analyses which often find that the direct knockout contribution can be quite small compared to the data and that meson exchange corrections can be important. The present study suggests that meson exchange current contributions may not be as large when treated in a relativistic framework. We also point out some difficulties we encountered in analyzing the data for a ^{12}C target at photon energies below 80 MeV.

1 Introduction

The reaction mechanism leading to the knockout of a single proton by a real photon has been the subject of some debate recently. Some nonrelativistic analyses [1, 2, 3, 4] suggest that the direct knockout (DKO) contribution may be very small compared to the data. Accordingly it was concluded that meson exchange current (MEC) contributions must be the main mechanism responsible for the observed cross sections. Similar conclusions were reported earlier for the nonrelativistic analyses carried out by Miller *et al.* [5] for ground state transitions for the reaction $^{16}\text{O}(\gamma, p)^{15}\text{N}$ at 60 and 72 MeV, and by Ireland *et al.* [6] for (γ, p) reactions on several nuclei for E_γ near 60 MeV (the same nuclei involved in the discussion reported in Ref. [1]). The above conclusions do not seem consistent with the findings by Ryckebusch *et al.* [7]. These authors find MEC effects to be relatively small for ground state transitions. The above statements illustrate the existing difficulty of arriving at a consensus within the nonrelativistic framework as to the extent of contributions from processes beyond simple direct knockout to ground state transitions in (γ, p) reactions. Although the differing views stated above appear to be somewhat dependent on the nuclear models used in the nonrelativistic calculations, they are, however, symptomatic of our incomplete understanding of the nature of the reaction mechanism for photonuclear reactions.

These results are quite different from those of a recent relativistic analysis of Johansson *et al.* [8] who find that, for an incident photon energy of 60 MeV, the DKO contribution accounts for most of the observed data, with no indication of any systematic sharp deviation from the data at this energy.

In this paper we extend the analysis reported in Ref. [8], for a photon energy of 60 MeV, to a much wider range of data. We consider several data sets for the (γ, p) reaction [and some data on the inverse reaction (p, γ)] on a number of target nuclei and covering a range of photon energies extending well into the Δ -resonance region. The spectroscopic factors and wave functions used in the calculations are fixed at the values obtained from a parallel analysis of the $(e, e'p)$ reaction on the same target nuclei. The objective of this study is to use this type of constrained analysis to gain some insight into the role of the DKO mechanism and to see if a consistent description of the available data is possible.

Section 2 outlines the relativistic calculations for the direct knockout

contribution to the (γ, p) reaction. Results of the calculations and details of the comparisons with data are given in section 3. Our conclusions are given in section 4.

2 Relativistic Calculations

The differential cross section due to the direct knockout contribution to the (γ, p) reaction has been given previously [8, 9] but we provide it here again for ease of reference. The relativistic expression for the differential cross section leading to a specific final state of the residual nucleus can be written as

$$\frac{d\sigma}{d\Omega_p} = \frac{\alpha}{4\pi} \frac{Mc^2}{\hbar c} \frac{|\mathbf{p}_p|^c}{E_\gamma} \frac{c}{v_{rel}} \frac{1}{R} \frac{\mathcal{S}_{J_i J_f}(J_B)}{2J_B + 1} \sum_{\mu M_B r} |\epsilon_r^\beta N_\beta^{\mu M_B}|^2 \quad (1)$$

where M_B and μ are the spin projections of the bound and continuum protons. We denote the four-momentum of the final proton p_p and the four-momentum of the incident photon as q . The four-vector ϵ_r^β is the photon polarization vector with two polarization states r , and summation is implied over repeated greek indices. The recoil factor R is given in any frame by [10]

$$R = 1 - \frac{E_p}{E_R} \frac{1}{|\mathbf{p}_p|^2} \mathbf{p}_p \cdot \mathbf{p}_R. \quad (2)$$

The four-momentum of the recoil nucleus is denoted by p_R . The function $N_\beta^{\mu M_B}$ is

$$N_\beta^{\mu M_B} = \int d^3x \Psi_\mu^\dagger(p_p, \mathbf{x}) \Gamma_\beta \Psi_{J_B, M_B}(\mathbf{x}) \exp(i\mathbf{q} \cdot \mathbf{x}), \quad (3)$$

where the wave functions of the continuum and bound nucleons, denoted Ψ_μ and Ψ_{J_B, M_B} respectively, are solutions of the Dirac equation containing appropriate potentials [9]. The 4×4 matrix Γ_β , operating on the nucleon spinors, is given by

$$\Gamma_\beta = \gamma_0 \left[\gamma_\beta + \frac{i\kappa_p}{2M} \sigma_{\beta\nu} q^\nu \right]. \quad (4)$$

The ingredients of the model are basically the same as used in an analysis of light to medium weight nuclei at 60 MeV [8]: the bound state protons are

described by solutions of a Dirac equation containing the relativistic Hartree potentials of Blunden and Iqbal [11], while the final state continuum proton is described by solutions of a Dirac equation containing complex phenomenological optical potentials obtained from fits to proton elastic scattering data [12]. Given these potentials, the only parameters left to determine are the spectroscopic factors. For the light nuclei: ^{10}B , ^{12}C and ^{16}O , we have obtained the spectroscopic factors by fitting the results of our $(e, e'p)$ model [8, 13] to available data. The ^{208}Pb data are not suitable for analysis using this model because of the lack of Coulomb distortions for the incident and final electrons. The spectroscopic factors used in this case are those of Udias *et al.* [14] who have performed a relativistic analysis of the ^{208}Pb data.

In the following we show the results of our calculations compared to the experimentally determined cross sections for several nuclei covering a wide energy range.

3 Results and Discussion

We have performed calculations for the (γ, p) reaction on several target nuclei, over a wide range of energies. These are compared to existing data in order to assess the extent to which the direct knockout mechanism contributes to the observed cross sections. The ingredients of the calculations have all been determined elsewhere and since there are no adjustments made, the results can be considered as predictions of the model.

In the graphs to be discussed below there are curves corresponding to several different calculations. The description of the calculations represented by each of these curves is as follows:

1. dashed curve — energy- (E -) dependent parameterization of the Dirac optical potentials specific to a single nucleus [12] while the bound state wave function is obtained through a Dirac-Hartree calculation [11];
2. dotted curve — E -dependent parameterization of the Dirac optical potentials specific to a single nucleus and the binding potential has a Woods-Saxon form;
3. solid curve — energy- and mass- $[(E+A)-]$ dependent parameterization of the Dirac optical potentials and the same Dirac-Hartree bound state wave function as in curve 1 above;

4. dot-dashed curve — curve 3 divided by a factor of 2.0 to bring the model calculations close to the data.

All the figures shown below use this designation of curves. The first three are simply for calculations using a variety of existing potential models in order to provide some feeling for the sensitivity of the results to variations in these ingredients. The dot-dashed curve is only relevant to graphs shown for the ^{12}C target.

3.1 ^{12}C Target

A considerable amount of data are available for this target. We have made comparisons of our relativistic DKO model calculations with these data, concentrating mainly on ground state transitions. These comparisons are shown in Figs. 1-3. Data for four of the energies shown in Fig. 1: $E_\gamma = 49.0, 58.4, 67.8$ and 78.5 MeV were reported by Springham *et al.* [15] and are obtained using the tagged photon facility at Mainz. The absolute magnitude of their cross sections was obtained by normalizing the data at each energy to data taken by Mathews *et al.* [16] for the (γ, p_{0+1}) reaction, data which include both the ground and first excited state of the residual ^{11}B nucleus. The data of Aschenauer *et al.* [17], at photon energies of $E_\gamma = 45.0$ and 54.0 MeV were obtained at the MAX-Lab at the University of Lund. These data were normalized completely independently of any previous experiment, and found to be consistent with existing data within systematic errors. The data at $E_\gamma = 73.5$ MeV from Rauf [18] were also obtained at the MAX-Lab. These data were normalized to previous measurements including those of Mathews *et al.* [16].

The most obvious feature apparent in Fig. 1 is that the calculations tend to form a narrow band lying above the data. Note that there is not much sensitivity to reasonable variation of the ingredients of the model. The light dot-dashed curve in all the figures shows the solid curve divided by a factor of 2, and this brings the curve close to the data in all cases. The calculated curves have the correct shapes and the variation of magnitude with incident photon energy also seems to be correct, but the curves lie consistently above the data by a factor of 2.

Figure 2 shows the differential cross section as a function of photon energy for four different proton angles. The experimental data are taken from

Ruijter *et al.* [19]; the experiments were also performed at the MAX-Lab at the University of Lund. Absolute normalization of these data was obtained independent of any other experiment and the results were found to be consistent with a large amount of other data. Again the calculated curves lie above the data by close to a factor of 2. We see that for photon energies above 40 MeV the energy and angular dependence are quite well reproduced by our model, but results lie above the data by a factor of 2.

In an attempt to compare to other data as well, we consider two experiments in which the first excited state of ^{11}B at 2.12 MeV ($1/2^-$) could not be resolved from the ground state. The experiment of Mori *et al.* [3] was performed at the Laboratory of Nuclear Science at Tohoku University. The experiment of Harty *et al.* [20] was performed at Mainz. The differential cross sections of both experiments were normalized without reference to any other experimental results and found to be consistent with other data. In order to compare to some data which do not contain the first excited state, ground state data from other sources were multiplied by a factor of 1.27 by both groups. This factor is assumed to account for population of the first excited state in ^{11}B being $\sim 27\%$ as probable as population of the ground state over the range of energies considered in both experiments. We adopt this factor in what follows.

In the left-hand column of Fig. 3 we show the measured energy distributions of Mori *et al.* [3] as the circular data points. The triangular points are taken from the data of Harty *et al.* [20]. The angles at which these data were taken do not coincide with the angles of the experiment by Mori *et al.*. For this reason the triangles shown at 66.0° represent cross sections which have been averaged for proton angles of 63.3° and 68.4° , while on the graph labeled 91.1° we show data averaged for 88.5° and 93.5° . Note that the 88 MeV data point of Harty *et al.* lies almost on top of the 87.8 MeV data point of Mori *et al.* showing the consistency between the two data sets. The curves are calculated assuming that the recoil nucleus is left in its ground state, and then multiplied by 1.27. The curves again lie above the data by a factor of 2 at low photon energies, but at the higher energies of the Mainz experiment the calculations seem to move closer to the data.

The right-hand column of Fig. 3 shows the angular distributions obtained by Harty *et al.* [20] compared to calculations as discussed in the previous paragraph. As the energy of the incident photons increases, the calculations seem to move from lying above the data by about a factor of 2, to falling

within the error bars for the data at the highest energy. Of course, because of the large error bars at larger proton angles the trend is not definitive, but it is suggestive.

The picture that is emerging for the status of the comparisons for the ^{12}C case can be further clarified by looking at the data available for (p, γ) reactions on this nucleus as well as those leading to its formation as a residual nucleus. The data are those obtained recently by Bright *et al.* [21] at Uppsala. Figure 4 shows comparisons to the data at proton energies of 98 and 176 MeV for ground state transitions to ^{12}C and ^{13}N residual nuclei. The former reaction is the inverse of the (γ, p) reactions discussed above. The comparisons for the ^{12}C residual nucleus are shown on the right hand side of the figure. Using the same wave functions and spectroscopic factors as in Fig. 1, we find that the calculations for $T_p = 98$ MeV lie slightly above the data at all angles except for the last point at $\theta_p = 140^\circ$. At 176 MeV the calculations are closer to the data except for the large angles. Thus the data for the inverse reaction confirm the behavior alluded to above; at lower energies the calculations seem to overestimate the cross sections.

The comparisons on the left-hand side of Fig. 4 present a somewhat different picture. Using the maximum value for the spectroscopic factor, the relativistic calculations for radiative capture on ^{12}C are close to or below the data. With a more realistic value of the spectroscopic factor the calculations will be further reduced in magnitude. This situation is in clear contrast to the cases discussed above. It should be noted, however, that with a spectroscopic factor in the range 0.5–1.0 (the maximum possible value is 1.0 in this case), the contributions of the knockout mechanism to the reaction are substantial in the region of lower missing momenta.

It is worthwhile to point out here that there are also unresolved difficulties for the ^{12}C target in the $(e, e'p)$ reaction, in addition to the difficulties discussed in the current work. The data from NIKHEF [22] are for kinematics with a fixed final proton kinetic energy of $T_p = 70$ MeV and nonrelativistic calculations shown in that paper cannot reproduce the shape of the distribution in missing momentum. In particular when the calculations are scaled to fit the peak for positive missing momenta, the calculations fall below the data for negative missing momenta. Our relativistic calculations show exactly this behaviour and the spectroscopic factor that we have used in this work is obtained by matching to the positive missing momentum peak. A proposed solution to this problem was to adjust the ratio of transverse to

longitudinal response functions, and when this ratio was adjusted to ≈ 1.3 [22] the shape of the missing momentum distribution was reproduced. This problem was considered further by van der Steenhoven [23] who found no justification for this enhancement factor. The newer data from Mainz on this nucleus, reported by Blomqvist *et al.* [24] have a higher final proton kinetic energy of $T_p \approx 90$ MeV. In this case, with the increase in normalization of the data by a factor of 1.19 [25], both nonrelativistic and our relativistic calculations can describe the shape of the measured missing momentum distribution using the spectroscopic factor as obtained from matching to the positive missing momentum peak of the NIKHEF data. This behaviour is consistent with the current results for the (γ, p) reaction on this nucleus: at low final proton energies model calculations differ from the data and as the final proton energy increases the calculations move closer to experimental results.

The data for proton knockout from the $1p_{3/2}$ orbital in ^{12}C seem to indicate that at low energies a simple shell model description is not adequate to explain the data. A more complete description might possibly involve inclusion of the deformed nature of the ground state wave function through a configuration mixing picture.

3.2 ^{10}B Target

Data for both the $(e, e'p)$ and (γ, p) reactions has been obtained for a ^{10}B target by de Bever [26] at two different energies. The data for knockout of a $1p_{3/2}$ proton leading to the ground state of ^9Be are shown in Fig. 5. Spectroscopic factors were obtained by scaling the model calculations to the $(e, e'p)$ momentum distribution (or reduced cross section) data for the $T_p = 70$ MeV case. The other $(e, e'p)$ and (γ, p) curves were then calculated without any adjustment of the parameters. It should be noted that the optical potentials used here are parameterized using proton elastic scattering data on targets from ^{12}C to ^{208}Pb . As a result of a lack of proton elastic scattering data on ^{10}B , we simply extrapolate the (E+A)-dependent potentials for use with a target lighter than ^{12}C . The (γ, p) calculations for this nucleus are quite sensitive to changes in the potentials used to generate the nuclear wave functions. In spite of this, and the fact that ^{10}B is not a closed shell nucleus, the DKO clearly produces results in the neighbourhood of the data.

3.3 ^{16}O Target

Figure 6 shows the differential cross section as a function of proton angle for knockout of a valence proton from an ^{16}O target, leading to the ground state of ^{15}N . The photon energy range is the largest available, with eight energies in the range $60 \text{ MeV} \leq E_\gamma \leq 361 \text{ MeV}$. The data come from three sources: Miller *et al.* [5] provide data points at energies of 60 and 72 MeV, while data shown at 60, 80 and 100 MeV are from Findlay and Owens [27]. The high energy data for photons in the range $196 \text{ MeV} \leq E_\gamma \leq 361 \text{ MeV}$ are from Adams *et al.* [28]. At low energies the calculated curves are generally close to the data, reproducing the magnitude and shapes quite well. For the higher energy data of Adams *et al.* the calculations tend to be close to the data points at small angles while falling below the data as the proton angle increases. This is the behavior one expects if meson exchange processes are going to become important as the missing momentum increases.

In order to remove some of the kinematic dependence from these curves we have calculated a *reduced cross section* by dividing the differential cross section of Eq. (1) by a kinematic factor [29, 1]:

$$2\pi^2 \alpha \frac{|\mathbf{p}_p| E_p}{E_\gamma} \frac{1}{M^2} \left[|\mathbf{p}_p|^2 \sin^2(\theta_p) + \frac{1}{2} \kappa_p^2 E_\gamma^2 \right]. \quad (5)$$

Figure 7 shows the reduced cross section as a function of missing momentum for all the experimental data shown in Fig. 6, as well as additional data provided by Leitch *et al.* [30]. The curves are generated using the same ingredients as the solid curves of Fig. 6 but restricted to the kinematic range covered by the data. An interesting observation here is that the model results are close to the data for missing momentum less than about 500 MeV/c. The vertical dotted line indicates the momentum of a free proton with kinetic energy equal to the charged pion mass. The calculations start to fall below the data in this kinematic region, which seems to be a good indication that we are seeing the need for inclusion of pion exchange diagrams to the reaction mechanism, and provides some idea of where these diagrams become important.

3.4 ^{208}Pb Target

Figure 8 shows results for proton removal from ^{208}Pb , leading to two doublets and one resolved state in ^{207}Tl , for two relatively low photon energies: 45 MeV and 54 MeV. The data are from Bobeldijk *et al.* [2]. These authors performed a nonrelativistic distorted-wave impulse approximation (DWIA) analysis of the data and found that the DKO contribution tends to lie up to a factor of 10 below the data. Revised recent analyses [17, 31] indicate that this factor may have been unrealistic. Our present analysis, on the other hand, shows that the relativistic calculations do come close to predicting the correct magnitudes of the observed cross sections. Within the parameter uncertainties, it is evident that the DKO mechanism is the leading contributor to the reaction at these energies.

4 Conclusions

In this paper we have presented relativistic calculations for the (γ, p) reaction and its inverse for a number of target nuclei. The results for the light targets cover a wide energy range, while the results for the lead target are at low energy but for a variety of final nuclear states. The analysis was done in a consistent manner with no free parameters. In all cases but one, $^{12}\text{C}(p, \gamma)$, the spectroscopic factor is obtained from a parallel analysis of the corresponding $(e, e'p)$ data.

In cases of transitions with simple nuclear structure, relativistic calculations indicate that the DKO mechanism is the main contributor to the cross section for lower missing momenta. For larger missing momenta one finds clear deviations indicating an increased role for higher order processes such as meson exchange and Δ -isobar contributions.

Nonrelativistic analyses often indicate that the contributions from the DKO mechanism are small and that meson exchange effects are sometimes dominant even at lower energies. In contrast, the present relativistic analysis suggests substantial contributions from the DKO mechanism to the cross sections over a wide range of energies. The analysis also points out that meson exchange effects are required at higher missing momenta.

In the course of this analysis we have found that in the case of the ^{12}C target for photon energies below 80 MeV, the relativistic calculations appear

to overestimate the cross section data by close to a factor of 2. This situation is puzzling and may indicate either some complications due to the structure of the ^{12}C nucleus itself or to some subtleties in the combined analysis of $(e, e'p)$ and (γ, p) for this target. It must also be noted that these difficulties do not occur for the spherical nuclei ^{16}O or ^{208}Pb , which are also considered in the present work. It is our feeling that the differences between theory and experiment at the lower proton energies for the ^{12}C target reflect the need for a proper description of the structure of this nucleus to include the intrinsic ground state deformation. The consistent approach based on a combined analysis of these two reactions [32, 1, 8] leads, in our view, to the conclusion that the ^{12}C ground state cannot be adequately described by simple single particle configurations.

In the case of transitions with simple structure (mainly single particle) our calculations indicate that meson exchange effects will not be important until one reaches missing momentum near 500 MeV/ c . With the effort to push $(e, e'p)$ reactions towards this region of missing momentum it would be interesting to see how important MEC effects will turn out to be in the relativistic model. Van der Sluys *et al.* [33] have considered this question in a nonrelativistic random phase approximation (RPA) framework and found large contributions from MEC's for larger missing momenta.

One point of interest is that the reactions discussed, $(e, e'p)$ and (γ, p) , show different sensitivities to the description of the bound state. This is probably due to the different range of missing momenta sampled by the two reactions. The $(e, e'p)$ reaction has been primarily concerned with low missing momenta where the bound wave function is constrained by properties such as binding energy and rms radius. The bound state wave functions that we use show little difference in momentum space for small momenta, and so it is not surprising that the $(e, e'p)$ results are very similar in this region. Differences between the bound state wave functions do arise, however, for larger missing momenta in $(e, e'p)$ and for the inherently large missing momentum reaction (γ, p) . This is not a surprise because this is where the nuclear wave function is poorly constrained and the region where we see differences between these bound state wave functions in momentum space.

A common criticism of the distorted-wave Born approximation (DWBA) approach, both relativistic and nonrelativistic, is the lack of orthogonality of the bound and continuum wave functions. It is argued that this lack of orthogonality could invoke spurious contributions to the cross sections. The

distorted continuum wave function is an approximation to the many-body wave function of the nuclear system with appropriate boundary conditions. This approximation derives its support from the fact that the wave function is constrained by proton-nucleus elastic scattering data. Nonrelativistic RPA calculations do not suffer from this lack of orthogonality, but the wave functions are not able to account for the elastic scattering data. A simple method for restoring orthogonality has been suggested by Boffi *et al.* [34] and Ciofi Degli Atti *et al.* [35]. These authors find the orthogonality effects to be relevant mainly at large angles. It is likely that this feature will carry over into the relativistic calculations and hence would not substantially change the main characteristics of the present calculations.

The present results pose certain challenges for the relativistic approach. If the DKO contributions are large then the data would suggest that the MEC effects are suppressed in the relativistic models, at least at the lower energies. Relativistic models must explain this suppression and in the meantime face the challenge of accounting for the observed relatively large photoneutron cross sections.

Spin-dependent observables are likely to play an important role in clarifying the reaction mechanisms. It should be noted here that the cross section angular distributions for (γ, p) reactions do not have much structure in most cases. The differences between competing models are then mainly differences in magnitudes, and hence may be related to normalization uncertainties in the models. When we discuss spin-dependent observables these normalization uncertainties cancel out and hence a better test of the model is likely to result.

Acknowledgments

One of us (H.S.S.) would like to thank the members of the Institute for Nuclear Theory at the University of Washington for their warm hospitality. We would like to thank Derek Branford for providing us with the data contained in Rauf's thesis [18] and for generously giving us permission to show them before publication. We are also grateful to L.J. de Bever and E.C. Aschenauer for allowing us to use their data before publication.

References

- [1] D.G. Ireland and G. van der Steenhoven, Phys. Rev. C **49** 2182 (1994).
- [2] I. Bobeldijk *et al.*, Phys. Lett. B **356** 13 (1995).
- [3] K. Mori *et al.*, Phys. Rev. C **51** 2611 (1995).
- [4] G. van der Steenhoven and H.P. Blok, Phys. Rev. C **42** 2597 (1990).
- [5] G.J. Miller *et al.*, Nucl. Phys. **A586** 125 (1995).
- [6] D.G. Ireland *et al.*, Nucl. Phys. **A554** 173 (1993).
- [7] J. Ryckebusch, K. Heyde, L. Machenil, D. Ryckbosch, M. Vanderhaeghen and W. Waroquier, Phys. Rev. C **46** 829 (1992).
- [8] J.I. Johansson, H.S. Sherif and G.M. Lotz, Nucl. Phys. **A605** 517 (1996).
- [9] G.M. Lotz and H.S. Sherif, Phys. Lett. B **210** 45 (1988); and Nucl. Phys. **A537** 285 (1992).
- [10] S. Frullani and J. Mougey, in *Advances in Nuclear Physics*, edited by J.W. Negele and E. Vogt, (Plenum Press, New York, 1984) Vol. 14, p. 1.
- [11] P.G. Blunden and M.J. Iqbal, Phys. Lett. B **196** 295 (1987);
P.G. Blunden, in: *Relativistic Nuclear Many-Body Physics*, edited by B.C. Clark, R.J. Perry and J.P. Vary (World Scientific, Singapore, 1989), p. 265.
- [12] E.D. Cooper, S. Hama, B.C. Clark and R.L. Mercer, Phys. Rev. C **47** 297 (1993).
- [13] M. Hedayati-Poor, J.I. Johansson and H.S. Sherif, Phys. Rev. C **51** 2044 (1995).
- [14] J.M. Udias, P. Sarriguren, E. Moya de Guerra, and J.A. Caballero, Phys. Rev. C **53** 1488 (1996).
- [15] S.V. Springham *et al.*, Nucl. Phys. **A517** 93 (1990).

- [16] J.L. Matthews, D.J.S. Findlay, S.N. Gardiner and R.O. Owens, Nucl. Phys. **A267** 51 (1976).
- [17] E.C. Aschenauer *et al.*, Nucl. Phys. (to be published).
- [18] A.W. Rauf, Ph.D. thesis, University of Edinburgh, 1996.
- [19] H. Ruijter, J-O. Adler, B-E. Andersson, K. Hansen, L. Isaksson, B. Schröder, J. Ryckebusch, D. Ryckbosch, L. van Hoorebeke and R. van de Vyver, Phys. Rev. C **54** 3076 (1996).
- [20] P.D. Harty *et al.*, Phys. Rev. C **51** 1982 (1995).
- [21] T.B. Bright, B. Höistad, R. Johansson, E. Traneus and S.R. Cotanch, Nucl. Phys. **A603** 1 (1996).
- [22] G. van der Steenhoven, H.P. Blok, E. Jans, M. de Jong, L. Lapikás, E.N.M. Quint and P.K.A. de Witt Huberts, Nucl. Phys. **A480** 547 (1988).
- [23] G. van der Steenhoven, Nucl. Phys. **A527** 17c (1991).
- [24] K.I. Blomqvist *et al.*, Z. Phys. A **351** 353 (1995).
- [25] J. Friedrich, Mainz, Germany, (1996) private communication.
- [26] L.J. de Bever, Ph.D. Thesis, Universiteit Utrecht, 1993.
- [27] D.J.S. Findlay and R.O. Owens, Nucl. Phys. **A279** 385 (1977).
- [28] G.S. Adams, E.R. Kinney, J.L. Matthews, W.W.Sapp, T.Soos, R.O. Owens, R.S. Turley and G. Pignault, Phys Rev C **38** 2771 (1988).
- [29] S. Boffi, C. Giusti and F.D. Pacati, Nucl. Phys. **A359** 91 (1981);
- [30] M.J. Leitch, J.L. Matthews, W.W. Sapp, C.P. Sargent, S.A. Wood, D.J.S. Findlay, R.O. Owens and B.L. Roberts, Phys. Rev. C **31** 1633 (1985).
- [31] E.C. Aschenauer, I. Bobeldijk, D.G. Ireland, L. Lapikás D. Van Neck, B. Schröder, V. Van der Sluys, G. van der Steenhoven and R.E. Van de Vyver, Phys. Lett. B **389** 470 (1996).

- [32] D.J.S. Findlay and R.O. Owens, Nucl. Phys. **A292** 53 (1977).
- [33] V. Van der Sluys, J. Ryckebusch, and W. Waroquier, Phys. Rev. C **54** 1322 (1996).
- [34] S. Boffi, R. Cenni, C. Giusti and F.D. Pacati, Nucl. Phys. **A420** 38 (1984).
- [35] C. Ciofi Degli Atti, M.M. Giannini and G. Salmè, Il Nuovo Cimento A **76** 225 (1983).

Figure Captions

FIG. 1. Knockout of a $1p_{3/2}$ proton from a ^{12}C target leading to the ^{11}B ground state. Angular distributions for seven different photon energies ranging from 45 to 78.5 MeV. Hartree bound state wave functions are used [11] and the proton optical potentials are from Ref. [12]. The data are from Refs. [15], [17] and [18]. Curves as discussed in the text.

FIG. 2. Knockout of a $1p_{3/2}$ proton from a ^{12}C target leading to the ^{11}B ground state. Distributions in photon energy at four fixed proton angles: $\theta_p = 30.0^\circ, 60.0^\circ, 90.0^\circ$ and 120.0° . The data are from Ref. [19]. Curves as discussed in the text.

FIG. 3. Knockout of a $1p_{3/2}$ proton from a ^{12}C target leading to the ^{11}B ground and first excited states. Left-hand column — distributions in photon energy at four fixed proton angles: $\theta_p = 30.6^\circ, 45.8^\circ, 66.0^\circ$ and 91.1° . Right-hand column — angular distributions for five photon energies. The data are from Refs. [3] and [20]. Curves as discussed in the text.

FIG. 4. Differential cross section as a function of photon angle for the (p, γ) reaction on ^{12}C and ^{11}B leading to the ground state. Curves as discussed in the text. The data are from Bright *et al.* [21].

FIG. 5. Single proton removal from the ^{10}B target leading to the ground state in ^9Be : upper figure — the $(e, e'p)$ reaction, lower figure — the (γ, p) reaction. Curves as discussed in the text. The data are from de Bever [26].

FIG. 6. Differential cross section as a function of proton angle for the knockout of a $1p_{1/2}$ proton from a ^{16}O target leading to the ^{15}N ground state. Curves as discussed in the text. The data are from Refs. [5, 27, 28].

FIG. 7. Reduced cross section as a function of missing momentum for the knockout of a $1p_{1/2}$ proton from a ^{16}O target leading to the ^{15}N ground state. Data as in Fig. 6 and from [30]. Curves as discussed in the text.

FIG. 8. Differential cross section as a function of proton angle for the knockout of protons from different levels in a ^{208}Pb target. Curves as discussed in the text. The data are from Bobeldijk *et al.* [2].

$$^{12}\text{C}(\gamma, p)^{11}\text{B}_{\text{g.s.}}$$

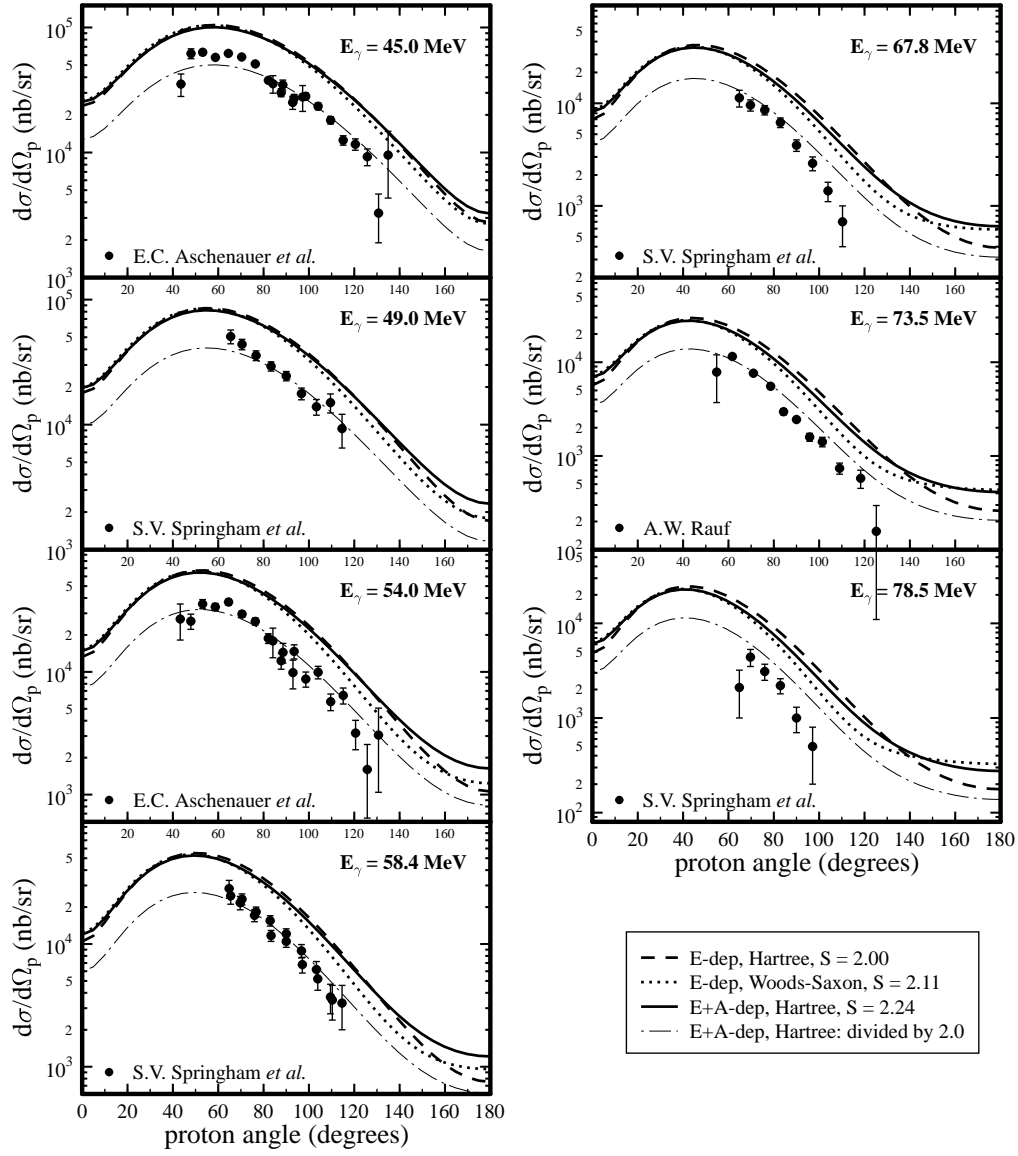


FIGURE 1.

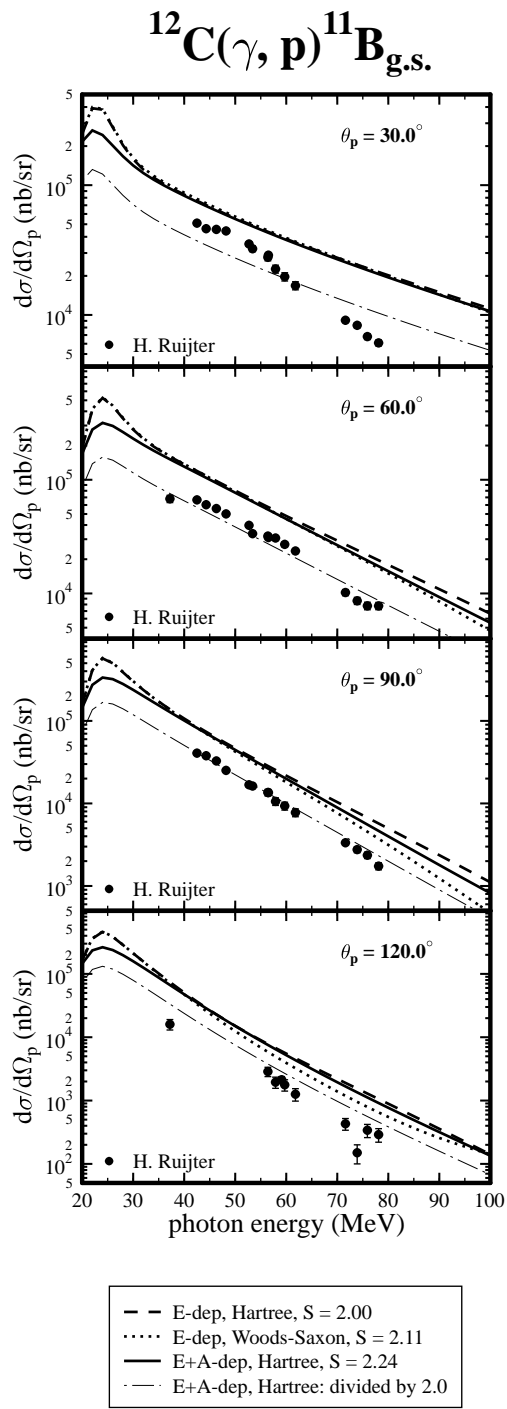


FIGURE 2.

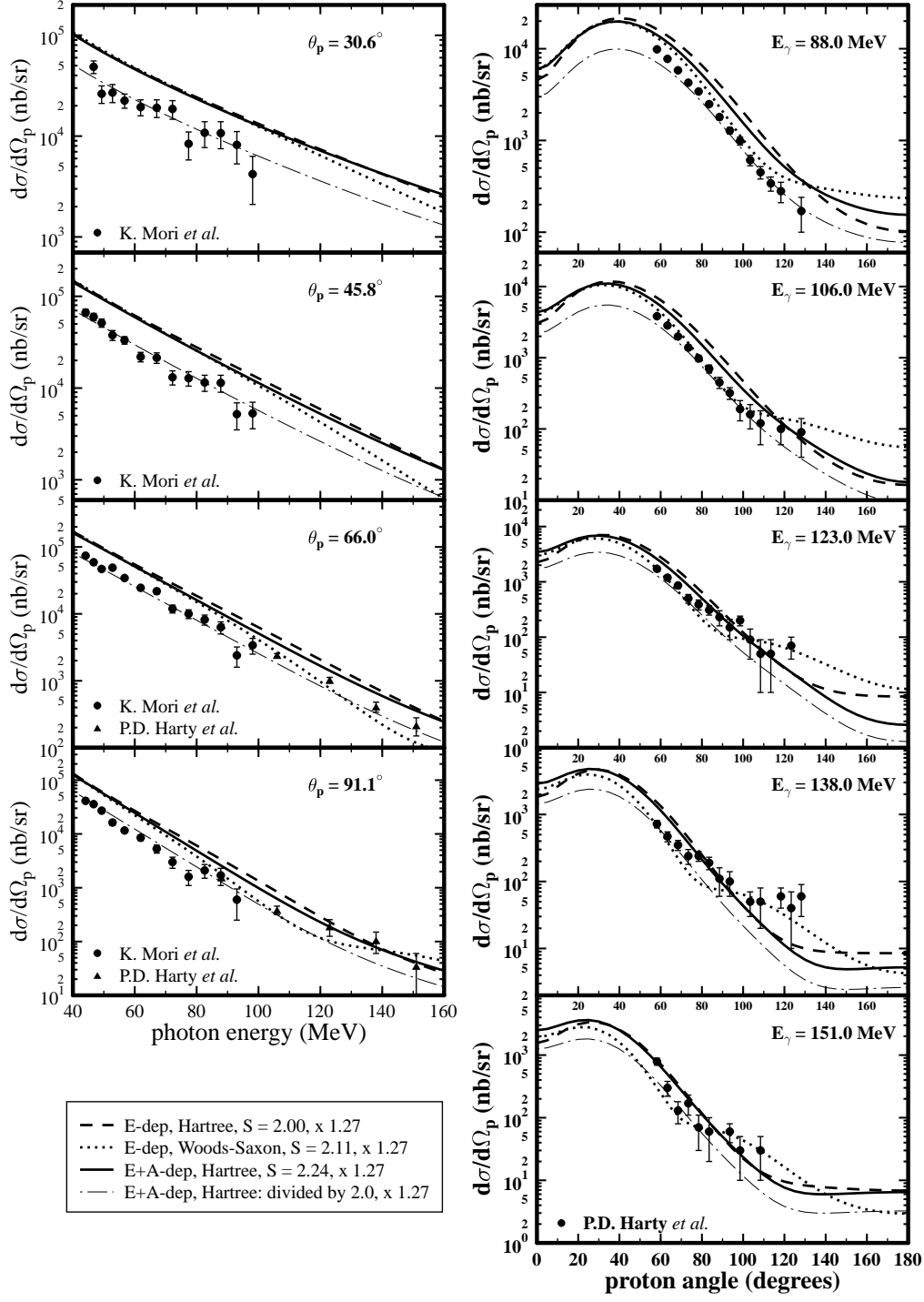


FIGURE 3.

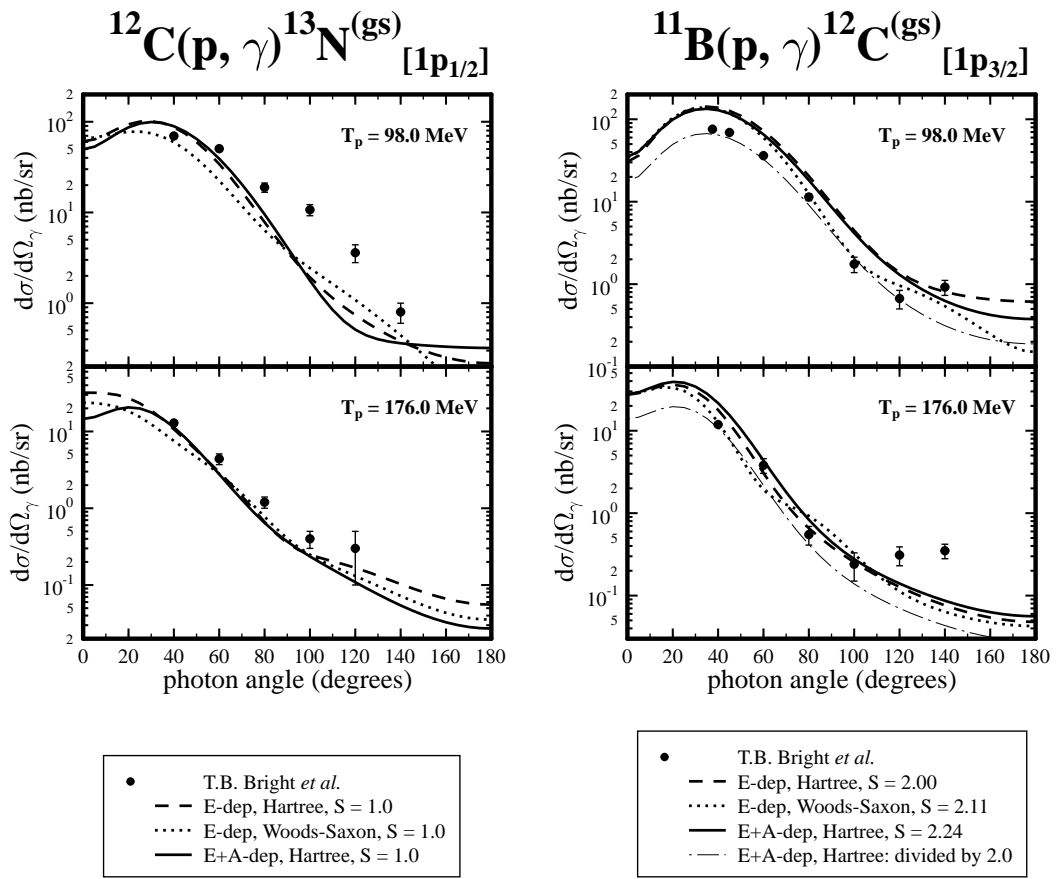


FIGURE 4.

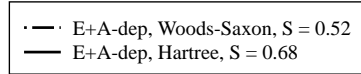
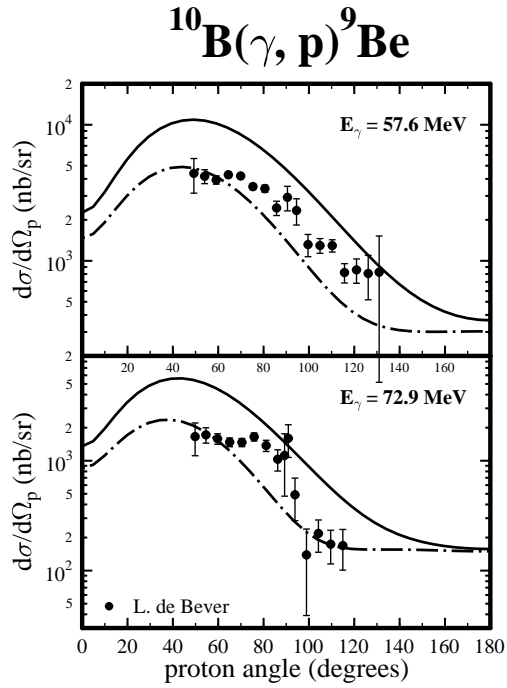
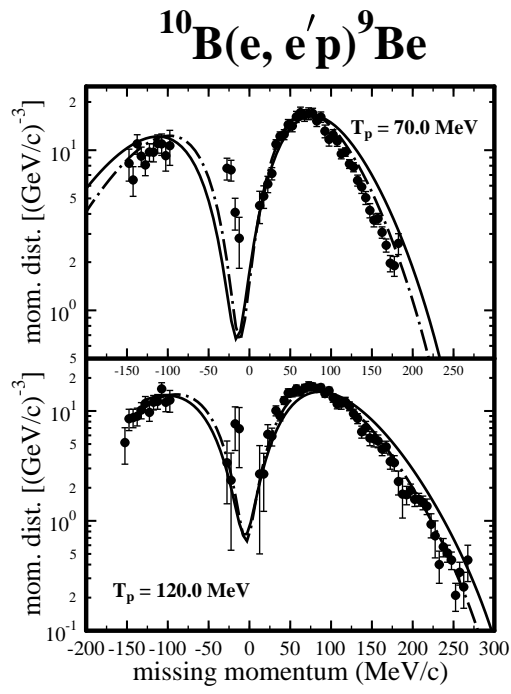


FIGURE 5.

$$^{16}\text{O}(\gamma, p)^{15}\text{N}_{\text{g.s.}}$$

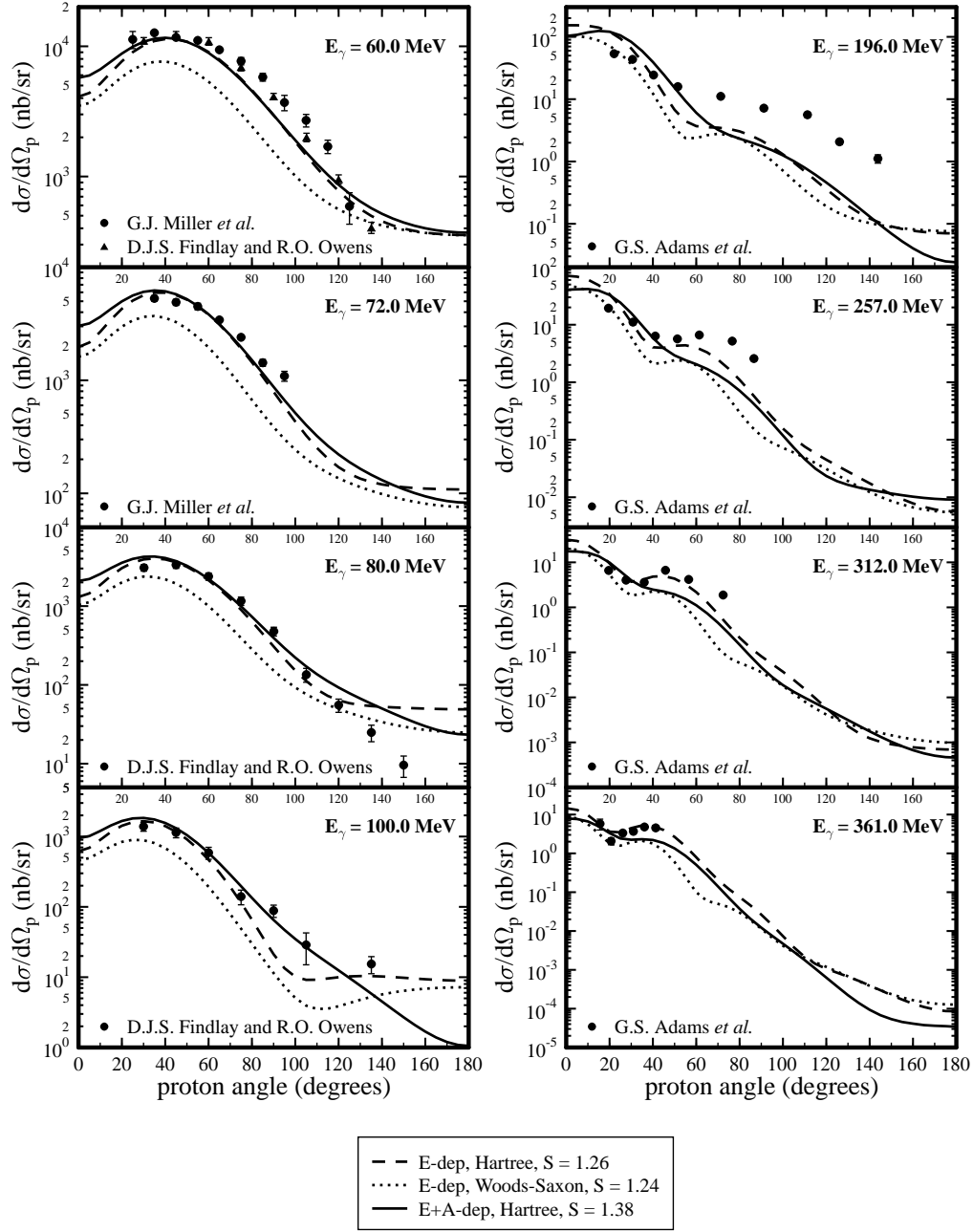


FIGURE 6.

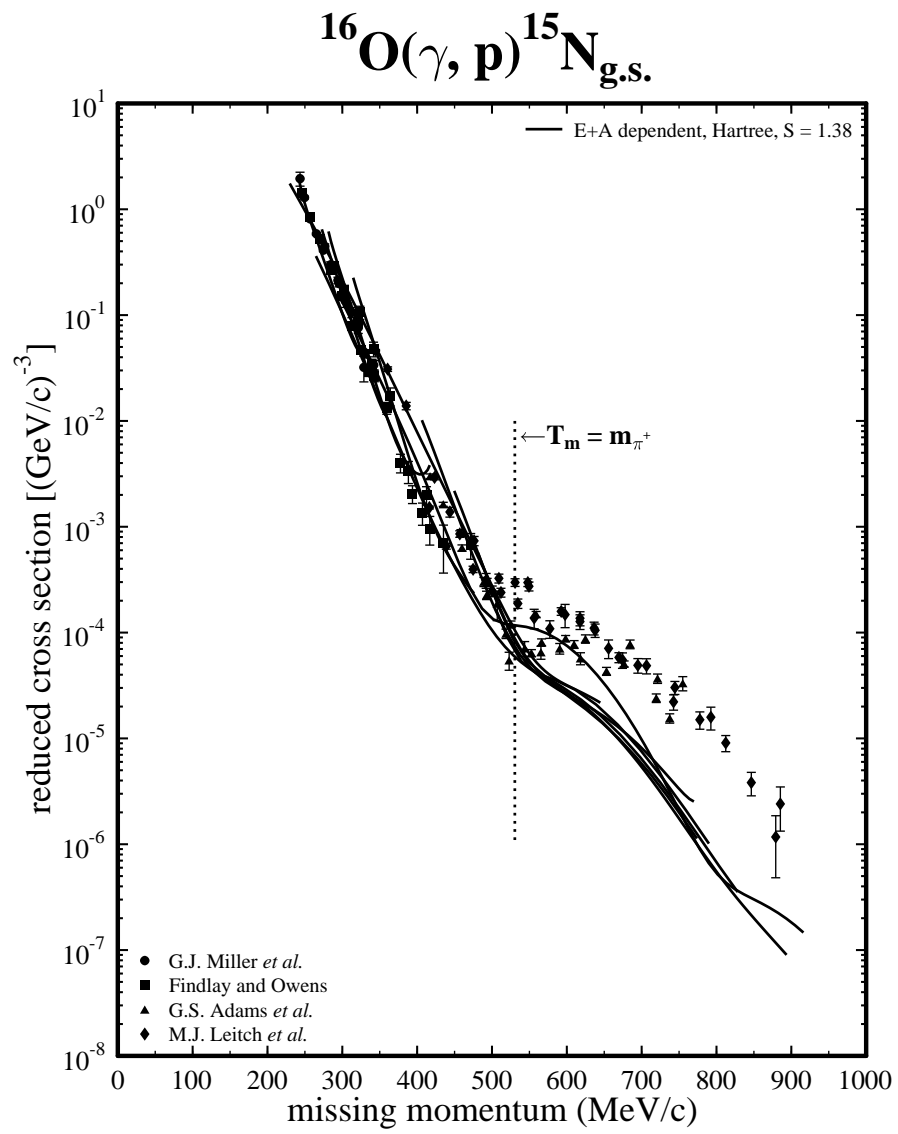


FIGURE 7.

$^{208}\text{Pb}(\gamma, p)^{207}\text{Tl}$

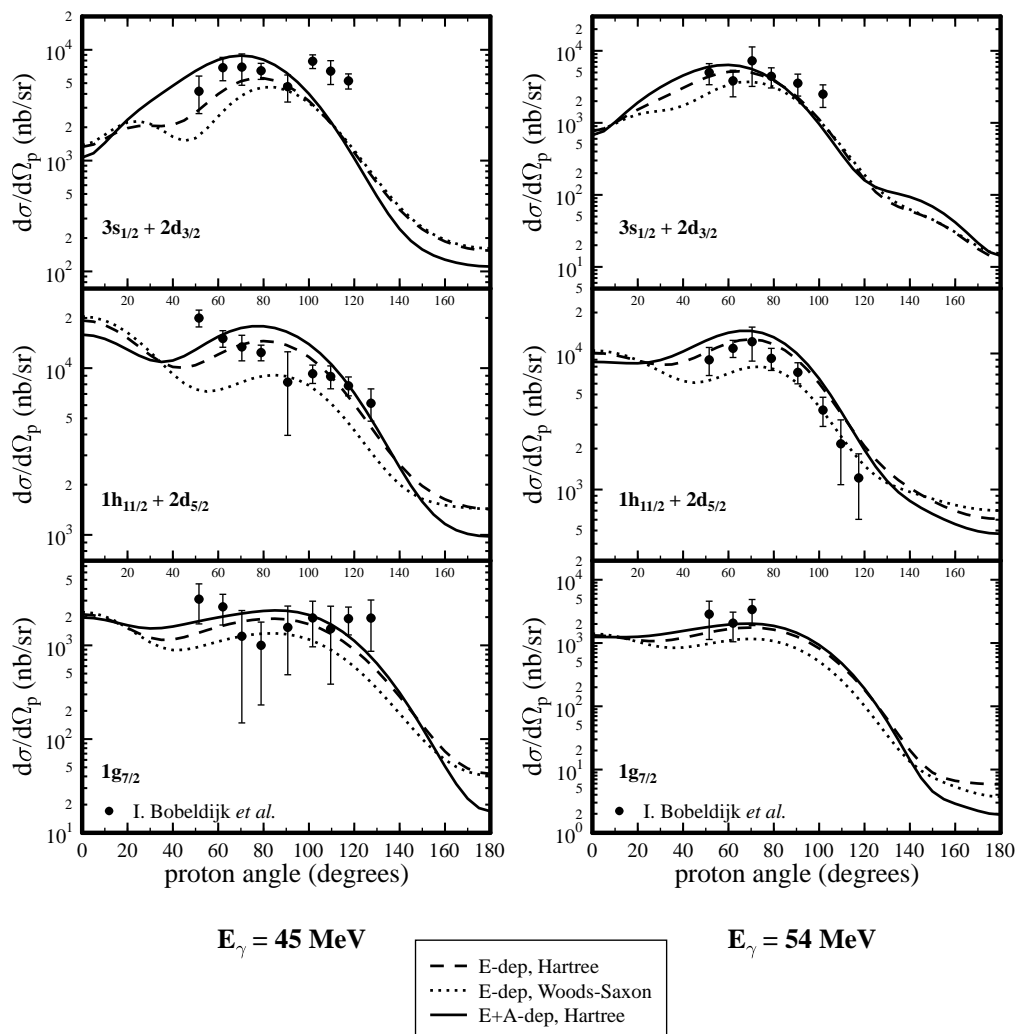


FIGURE 8.